NUEJ
Naresuan University Engineering Journal

Modeling Molecular Structural Properties of Magnetite (Fe_3O_4) and Mackinawite (FeS) Using Density Functional Theory (DFT)

Saranya Tongkamnoi [1,*], Mayuree P. Reilly [2], Tanapon Phenrat [1,3*]

[1] Research Unit for Integrated Natural Resources Remediation and Reclamation (IN3R), Department of Civil Engineering, Faculty of Engineering, Naresuan University, Phitsanulok, Thailand, 65000
[2] College of Materials Innovation and Technology, King Mongkut's Institute of Technology Ladkrabang, Rd., Ladkrabang, Bangkok, Thailand, 10520
[3] Center of Excellence for Sustainability of Health, Environment, and Industry (SHEI), Faculty of Engineering, Naresuan University, Phitsanulok, Thailand, 65000

*Corresponding author e-mail: pomphenrat@gmail.com

(Received: 30 May 2023, Revised: 27 November 2023, Accepted: 29 November 2023)

Abstract

Bare and sulfidized nanoscale zerovalent iron (bare NZVI or Fe^0 and S-NZVI, respectively) has been widely utilized for environmental restoration. During the degradation and sequestration of contaminants of concern (COCs) such as chlorinated organics and toxic metals, interfacial detoxification reactions are governed by the physical chemistry of the iron oxide shell of bare NZVI and the iron sulfide shell of S-NZVI: magnetite (Fe_3O_4) and mackinawite (FeS), respectively. Because interfacial reactions generally cannot be directly and experimentally monitored, this study examines first-principles methods based on the use of the density functional theory (DFT) as a simulation tool to help understand interfacial phenomena. In this study, DFT approaches with and without long-range van der Waals interactions (so-called DFT and DFT-D2 approaches, respectively) were employed. The simulated unit cell parameters and electronic density of states (DOS) of bulk Fe_3O_4 and FeS were modeled using both DFT and DFT-D2 methods and compared with previous experimental results where these were available. We reveal that there was strong agreement between the simulated properties and previous experimental results. Nevertheless, for both Fe_3O_4 and FeS, the DFT-D2 method performed better than the DFT method in terms of the accuracy of simulated unit cell parameters. Furthermore, the DFT-D2 method simulated the DOS of both materials effectively. The DOS of Fe_3O_4 supports electron transfer from the central octahedral-Fe_B layer to the outer tetrahedral-Fe_A layer, while the DOS of FeS potentially explains the decrease of the NZVI aging effect and enhanced treatment for hydrophobic contaminants due to sulfidation reported in literature. This research projects that DFT-D2 can be used as a tool of choice for understanding the interaction between COCs and Fe_3O_4 and FeS surfaces at nanoscale in order to develop the environmental applications of nanomaterials. For this purpose, further modification of the model is required to properly downscale the computation from bulk to nanoscale materials.

Keywords: density functional theory (DFT), electronic density of states (DOS), simulation, surface energy, Unit cell parameter.

1. NOMENCLATURE

DFT: Density functional theory
DFT-D2: Method combining the DFT energy with a correction to the long-range dispersion interactions
GGA: Generalized gradient approximation
KS: Kohn-Sham
LEED: Low energy electron diffraction
PAW: Projector augmented-wave
PBE: Generalized gradient approximation density functional developed by Perdew, Burke and Ernzerhof
STM: Scanning tunneling microscopy
VASP: Vienna Ab-initio Simulation Package
XPS: X-ray photoelectron spectroscopy
XRD: X-ray diffraction

2. INTRODUCTION

Nanoscale zerovalent iron (NZVI, or Fe^0) has been widely utilized for environmental restoration due to its high reactivity with halogenated organic pollutants, heavy metals, and other inorganic pollutants (Phenrat et al., 2016; Phenrat et al., 2018; Phenrat and Lowry, 2019). Nevertheless, as a side reaction between Fe^0 and

water in aquatic environments, NZVI oxidative aging results in unintended H_2 production and electron depletion and competes with intentional reactions for contaminant abatement (Liu et al., 2005; Liu et al., 2007; Mackenzie and Georgi, 2019; Phenrat and Lowry, 2019). NZVI aging leads to surface passivation and a short reactive lifetime unfavorable for environmental engineering applications due to the associated increase in material and operational costs. The main chemical reaction involved in NZVI aging is the oxidation of iron, which generally leads to the formation of a Fe(II)/(III) iron oxide shell. Magnetite (Fe_3O_4) is often a major oxide phase formed under anaerobic conditions. Intrinsic magnetic attraction caused by Fe_3O_4 is the dominant driving force for the agglomeration of NZVI, negatively affecting both suspension stability and transport in saturated porous media. Moreover, although Fe_3O_4 is widely used as the main component of industrial catalysts in numerous processes, there is no agreement on either the termination of its main surfaces or the thermodynamics of the redox reactions taking place on them (Reinsch et al., 2010) while the Fe^0 core is shrinking (Mackenzie and Georgi, 2019; Phenrat and Lowry, 2019). Thus, during the detoxification of chlorinated organics or the sequestration of toxic metals and metalloids in the subsurface using NZVI, contaminants of concern (COCs) will interact with the magnetite surface and not the Fe^0 surface. Consequently, understanding interfacial interactions between COCs and the Fe_3O_4 surface is important for the research and development of NZVI for engineering applications.

On the other hand, as an engineering attempt to alleviate the aging effect, sulfidation can be used to modify NZVI, resulting in the transformation of the NZVI surface to mackinawite (FeS). Sulfidized NZVI (S-NZVI) creates a nucleophilic zone on the particle surface with a lower density of H atoms compared to NZVI, which reduces the recombination of H atoms to form H_2 (water-induced corrosion). However, it enhances the β-elimination pathway for halogenated carbon compounds by facilitating the adsorption between positively charged carbons (α position) and the nucleophile (S^{2-})(Fan et al., 2016; Phenrat and Lowry, 2019). The FeS surface not only alleviates Fe^0 aging but also enhances reactivity and improves electron selectivity for targeted contaminants (Fan et al., 2016; Phenrat and Lowry, 2019). For example, during the dechlorination of chlorinated organics such as trichloroethene (TCE), S atoms on the FeS surfaces appear to induce the formation of acetylene through β-elimination, which consumes less electrons than the hydrogenolysis pathway (Su et al., 2019). Due to the high conductivity of FeS (Su et al., 2019), the dechlorination rate through β-elimination is accelerated. Furthermore, S results in low H atom density, which is not favorable for further hydrogenolysis of acetylene to ethene or ethane because the formation of ethene and ethane from acetylene occurs in high H atom density zones. This means that TCE dichlorination via S-NZVI consumes less electrons than via bare NZVI. Several mechanisms have been hypothesized for the enhanced reactivity and selectivity of S-NZVI compared to bare NZVI. First, S-NZVI is more hydrophobic than bare NZVI, resulting in less interaction with water and charged solutes and greater interaction with hydrophobic contaminants, such as chlorinated organics. Second, the incorporated sulfur lowers the electron transfer resistance of Fe^0 to the contaminant. Third, the incorporated sulfur blocks the adsorption sites for atomic hydrogen and inhibits the water reduction reaction and H_2 evolution (Xu et al., 2021).

These hypotheses have been proposed as a basis for the roles of NZVI aging and sulfidation in groundwater detoxification. Nevertheless, surface reactions are difficult to directly measure and quantify. For this reason, density functional theory (DFT), a form of molecular modeling, is a tool of choice to examine these hypotheses. The accuracy of the DFT is comparable with correlated molecular orbital methods but requires substantially less computational effort (Wimmer, 1996). Because of its computational advantages, DFT has evolved as the most important quantum mechanical approach in solid-state physics (Politzer et al., 1993; Dahl and Avery, 2013) and can handle large, periodic systems that are intractable when using correlated molecular orbital methods (Labanowski and Andzelm, 2012). In DFT, the energy is decomposed into contributions from kinetic energy, the Coulomb energy, and exchange-correlation energy. Although this decomposition is exact, its implementation requires approximations since the actual functionals for the many body exchange and correlation energies are unknown.

In this study, as the first step towards understanding bare and S-NZVI interfacial reactions at nanoscale, we examine the electronic and magnetic properties of bulk Fe_3O_4 and FeS via two different DFT tools and compare the modeling results with measurable parameters, where these are available, for calibration. In future studies, the calibrated model can be used as a base model for the modification and modeling of non-measurable phenomena at nanoscale for environmental nanotechnology applications.

3. COMPUTATIONAL METHODS AND MODEL EVALUATION

Atomistic model simulations based on Density Functional Theory (DFT) are undeniably the most popular quantum chemical methods for analyzing the

structure-property relationships of crystalline compounds. DFT has gained significant popularity in solid-state physics. The choice of the functional and basis set are the two most critical variables that must be determined before commencing DFT calculations, and this choice greatly influences the results obtained. Fig. 1 shows two DFT approaches were used for all calculations and optimizations in this study. First, we carried out spin-polarized quantum mechanical calculations PBE was performed using a uniform Monkhorst and Pack grid of 21 x 21 x 21 for sampling BZ and density of states (DOS), because it provides a better description of the structure of solids than its parent functional (De la Pierre et al., 2011). Second, we also using density functional theory (DFT) as implemented in the Vienna Ab-initio Simulation Package (VASP) (Kresse and Hafner, 1993; Kresse and Furthmüller, 1996). The Perdew-Burke-Ernzerh functional (PBE) (Perdew et al., 1992; Perdew et al., 1996) was the version of the generalized gradient approximation (GGA) used as the exchange correlation functional for all geometry optimizations and for the calculation of electronic band structure integration over the Brillouin zone (BZ). The utilized the DFT-D2 proposed by Grimme to model long-range van der Waals interactions (Grimme, 2006). Although these interactions were not expected to significantly affect the bulk properties of the hard solids investigated here, we included the D2 correction at this stage because in future work we expect to study the surfaces of these solids under interactions with COCs at nanoscale, where dispersion effects may play a significant role (Santos-Carballal et al., 2014; Santos-Carballal et al., 2018). The projector augmented wave (PAW) pseudopotential method (Blochl, 1994; Kresse and Joubert, 1999) was used to describe the core electrons and their interactions with the valence electrons, i.e. those in level Fe(3s, 3p, 3d, 4s) and Fe(2s, 2p). The kinetic energy cutoff for the planewave basis set expansion was set at 520 eV for the geometry optimizations, in order to avoid Pulay stress arising from the cell shape relaxations(Mackenzie and Georgi, 2019). The BZ was examined using 11 × 11 × 11 and 5 × 5 × 1 Monkhorst-Pack mesh k-points for bulk and surface calculations, respectively (Monkhorst and Pack, 1976). During relaxation, the energy convergence defining the self-consistency of the electron density was 10^{-5} eV, while the Feynman forces acting on each atom were minimized until they were < 0.01 eV/Å.

Nanomaterials and bulk materials are both fundamental particle types, but the key distinction between nanomaterials and bulk materials is their 'size.' Nanomaterials have dimensions ranging from 1-100 nanometers, at least in one dimension, whereas bulk materials have sizes greater than 100 nanometers in all dimensions. Furthermore, bulk materials exhibit periodic crystalline arrangements occurring periodically in an orderly manner, while nanomaterials lack such characteristics. In addition, they possess differing chemical and physical properties, leading to diverse applications. To simulate Fe_3O_4 (magnetite, *Fd3m* space group and octahedral structure), a cubic inverse spinel structure with a lattice constant of 8.396 Å and eight formula units ($Fe_{24}O_{32}$) was set as an initial structure (Weiss and Ranke, 2002; Yang et al., 2010). The O anions formed a close-packed face-centered cubic (FCC), which was sublatticed with $Fe^{2+}$and Fe^{3+} sites; one site in the tetrahedral coordinate was occupied only by Fe^{3+}, while the other sites in the octahedral coordinate were equally occupied by Fe^{3+} and Fe^{2+} ions. In this work, the magnetite model which used ionic cores was described by the ultrasoft pseudo potential (Vanderbilt, 1990). On the other hand, to simulate FeS (mackinawite, *P4/nmm* space group) (Lennie et al., 1995; Dzade et al., 2013; Dzade et al., 2014), a tetragonal structure consisting of two Fe and two S atoms (Berner, 1962) was set. A non-magnetic state was modeled in this study according to work by Devey et al. which revealed that the stable ground state of FeS is non-magnetic (Devey et al., 2008). This effect has been ascribed not only to the strong covalency of the Fe–S bond but also to extensive d-electron delocalization within the sheets (Vaughan and Ridout, 1971).

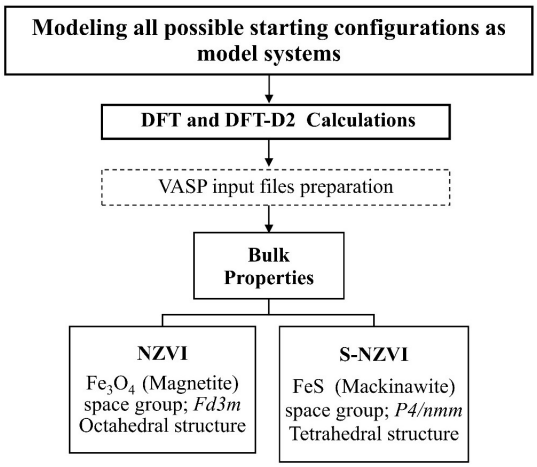

Figure. 1 Flowchart of all the DFT and DFT-D2 steps in this study

As for model evaluation, two major indicators were assessed. Lattice parameters and bond distances optimized by both simulation approaches for both bulk materials were compared with the measured lattice parameters and bond distances of the corresponding bulk materials as experimentally quantified using scanning tunneling microscopy (STM), low-energy electron diffraction (LEED) and X-ray photoelectron diffraction (XPD) in previous studies. While these DFT simulations yield graphical profiles of electron density in states at different energy levels, these profiles cannot be monitored experimentally; rather, only the energy band gap can be experimentally measured using a

photoconductive light detector. Thus, the simulated band gaps of the two DFT approaches were compared against the experimental band gap values. Understanding the entire electron density profiles at different energy levels is important, since this governs bulk properties such as specific heat, paramagnetic susceptibility, and other transport phenomena of conductive solids.

4. RESULTS AND DISCUSSION

4.1 Structural Properties of Fe_3O_4 and *FeS*

Fig. 2 demonstrates the simulated magnetite (Fe_3O_4) unit cells adhering to the face centered cubic pattern. It shows the presence of eight formula units (*z* parameter) within each magnetite unit cell. The super cell parameters optimized using the DFT and DFT-D2 methods are shown in Table 1.

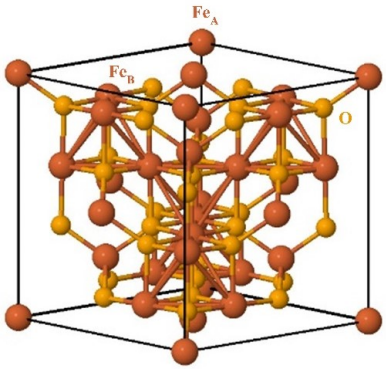

Figure. 2 Schematic illustration of bulk bare-NZVI (Fe_3O_4) Color scheme: Fe = brown and O = orange.

Notably, the super cell parameters optimized by both the DFT and DFT-D2 methods in this study substantially agree with previous experimental results obtained using STM, LEED and XPD (Barbieri et al., 1994; Kim-Ngan et al., 2004). Nevertheless, the super cell parameters optimized by DFT-D2 agree with the experimental results better than those optimized by DFT, suggesting that long-range van der Waals interactions are relevant for modeling magnetite structures. For example, the a = b = c values optimized by DFT-D2 and DFT were 8.324 Å and 8.533 Å, respectively, while the experimental a = b = c value was 8.396 Å. Similarly, the d(Fe_{tet}-O) values optimized by DFT-D2 and DFT were 1.850 Å and 1.939 Å, respectively, while the experimental d(Fe_{tet}-O) value was 1.880 Å. Finally, the d(Fe_{oct}-O) values optimized by DFT-D2 and DFTwere 2.079 Å and 2.082 Å, respectively, while the experimental d(Fe_{oct}-O) value was 2.070 Å.

Table 1 Optimized bulk structural parameters of magnetite (Fe_3O_4) compared with lattice parameters and bond distances from previous studies.

Unit cell parameters (Å)	**DFT**	**DFT-D2**	**Experimental** (Barbieri et al., 1994; Kim-Ngan et al., 2004)
a = b = c	8.533	8.324	8.396
d(Fe_{tet}-O)	1.939	1.850	1.880
d(Fe_{oct}-O)	2.082	2.079	2.070

In the simulated mackinawite (FeS) structure (Fig. 3), each iron atom was arranged in tetrahedral coordination with sulfur in a square lattice. This yielded edge-sharing tetrahedral layered sheets, which were stacked along the c-axis and stabilized via van der Waals forces (Dzade et al., 2013; Dzade et al., 2014). The sulfur atoms were positioned on the elongated sides of the unit cell. The super cell parameters optimized by DFT and DFT-D2 from this initial structure are shown in Table 2.

Notably, the super cell parameters optimized by both DFT and DFT-D2 in this study agree well with previous experimental results measured using XRD, TEM and XPS (Berner, 1962; Lennie et al., 1997; Jeong et al., 2008). Initially, we carried out geometry optimizations of the FeS structure without accounting for van der Waal forces (i.e., DFT only) and found that the interlayer spacing was overestimated. For example, the lattice parameters produced by DFT after a full geometry optimization converged to $a = b = 3.587$ Å, $c = 5.484$ Å, and c/a ratio = 1.529 Å, which is 12% greater than the c/a ratios; this compares well with the range of previous experimental values reported in Table 2.

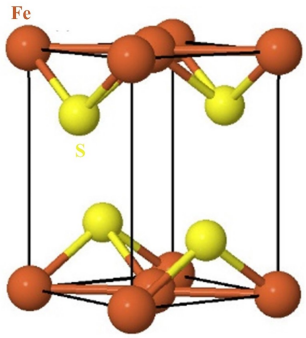

Figure. 3 Schematic illustration of bulk (a) S-NZVI (FeS). Color scheme: Fe = brown, S = yellow.

Nevertheless, as previously mentioned, standard DFT-based methods often result in poor estimation of the inter-layer spacing of most layered structures, including FeS. For this reason, by implementing the DFT-D2 method of Grimme to account for the weak

dispersion forces, we predicted the interlayer separation distance as 4.861 Å. This is only 3% lower on average than previous experimental results (Lennie et al., 1997), confirming the importance of this correction to include dispersion forces for an accurate prediction of the interlayer separation distance in FeS. Using the DFT-D2 theoretical method described above and allowing all atoms to fully relax until the required accuracy was reached, we calculated the unit cell parameters at a = b = 3.564 Å and c = 4.861 Å with c/a ratio = 1.364 Å, which compares well with the range of experimental values reported in Table 2 (Berner, 1962; Lennie et al., 1997; Jeong et al., 2008).

Table 2 Optimized bulk structural parameters of mackinawite (FeS) compared with lattice parameters and bond distances from previous studies.

Unit cell parameters (Å)	**DFT**	**DFT-D2**	**Experiment** (Lennie et al., 1997)
a = b	3.587	3.564	3.650
c	5.484	4.861	4.997
c/a	1.529	1.364	1.363
d(Fe-S)	2.160	2.156	2.240
d(Fe-Fe)	2.536	2.520	2.598

4.2 Electronic Structure of Fe_3O_4 and *FeS*

Band structure

Fig. 4 shows the electronic band structure of Fe_3O_4 in the *Fd3m* unit cell simulated by DFT-D2. Red lines show valance bands, while blue lines represent conduction bands. The X-axis illustrates the Brillouin zone (BZ), defined as a Wigner-Seitz primitive cell in the reciprocal lattice specified with systematic symbols of the cell, such as Z, R, and M points (Monkhorst & Pack, 1976), while the Y-axis illustrates the energy of the band (eV). This simulated result provides insight into several measurable or observable physicochemical characteristics of the materials. For example, Fig. 4 shows that the band gap was calculated as 0.82 eV, which is similar to the band gap measured by photoconductor (1.26 eV) (Marand et al., 2014). Moreover, the Z point in the X-axis shows a direct band gap where the valance band and the conduction band meet, confirming the pattern of a metal electronic structure, which is in good agreement with the metal nature of Fe_3O_4. The PBE results indicate that cubic Fe_3O_4 is a half-metallic oxide, with the majority spin band exhibiting insulating or semiconducting behavior and the minority spin band showing metallic behavior.

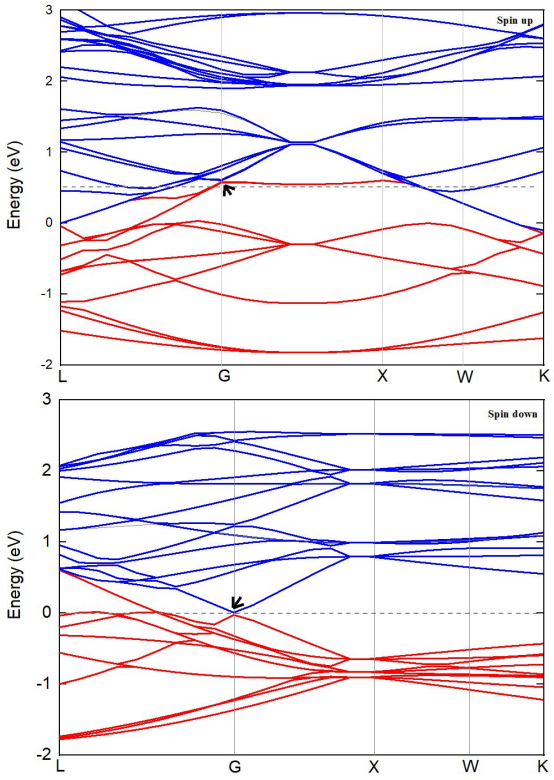

Figure 4 DFT-D2(PBE) electronic band structure of Fe_3O_4 in the *Fd3m* unit cell and. The partial charge density at valence band maximum or conduction band minimum (VBM or CBM, as indicated with an arrow). The Fermi level (=zero of energy, see text) is shown as a dashed line.

Fig. 5 shows the electronic band structure of FeS in the *P4/nmm* unit cell simulated by DFT-D2. Similar to the electronic band structure of Fe_3O_4, the red lines show valance bands while the blue lines represent conduction bands. Similarly, as shown in Fig. 5, the band gap was calculated as 0.60 eV, which is similar to the band gap measured by photoconductor (0.95 eV) (Sun et al., 2011). Moreover, the M point on the X-axis shows a direct band gap where the valance band and the conduction band meet, confirming the pattern of a metal electronic structure, which is in good agreement with the metal nature of FeS.

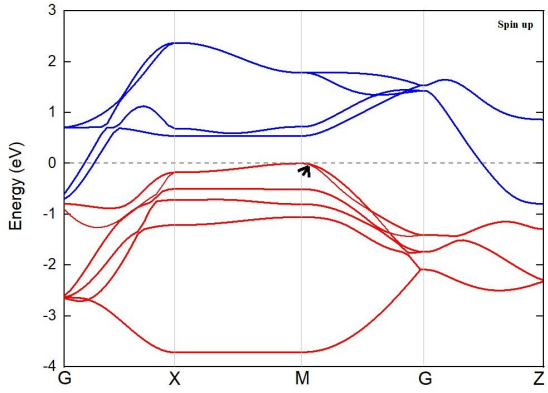

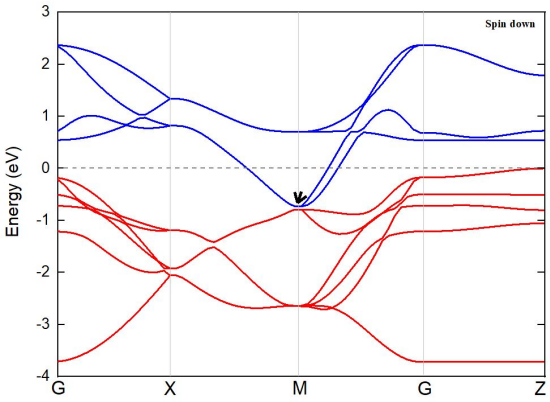

Figure. 5 DFT-D2(PBE) electronic band structure of FeS in the *P4/nmm* unit cell . The partial charge density at valence band maximum or conduction band minimum (VBM or CBM, as indicated with an arrow). The Fermi level (=zero of energy, see text) is shown as a dashed line.

Density of states (DOS)

Moreover, the simulation results also shed some light on phenomena which are technically difficult to directly examine. For example, it is technically challenging to measure electron transfer from Fe^0 through a Fe_3O_4 shell, especially for nanosized particles, but the DFT-D2 can simulate the electronic density of states (DOS) for bulk Fe_3O_4 (Fig. 6(a)), and this can be used to predict electron transfer potential across the iron oxide shell. Theoretically, electron transfer takes place when the energy of electrons in inner orbitals (E) minus the energy of valance electrons (E_f) becomes greater than the Fermi energy. At T = 0 K, the Fermi energy is equal to zero. Thus, according to Fig. 6(a), the DOS corresponding to $E-E_f > 0$ eV represents the electrons which can transfer from the central octahedral-Fe_B layer to the outer tetrahedral-Fe_A layer (Fig.1). Because DOS is essentially the number of different states at a particular energy level that electrons are allowed to occupy, i.e. the number of electron states per unit volume per unit energy, the DOS corresponding to $E-E_f > 0$ represents the number of electron states per unit volume per unit energy which can transfer from the inner orbitals of Fe_3O_4 (i.e., the central octahedral-Fe_B layer) to the outer orbital (i.e. the outer tetrahedral-Fe_A layer). Similarly, for the DOS corresponding to $E-E_f < 0$, electron transfer from the inner orbital to the outer orbital will not occur. In sum, the DOS results in Fig. 6 (b) reveal the potential for electron transfer across the Fe_3O_4, which cannot be experimentally measured.

Interestingly, the simulated DOS of FeS shown in Fig. 6(b) provides potential explanations for the decrease of the NZVI aging effect and enhanced treatment of hydrophobic contaminants by S-NZVI reported in the literature (Fan et al., 2016; Phenrat and Lowry, 2019). For Fe-d states, the DOS corresponding to $E-E_f > 0$ is less than $E-E_f < 0$, while for S-p states, the DOS corresponding to $E-E_f > 0$ is greater than $E-E_f < 0$, suggesting that electron transfer is more favorable through the S than through the Fe of the FeS (Fig. 3).

Thus, NZVI aging is decreased by the presence of FeS because there is less NZVI oxidation due to less electron transfer through the Fe. On the other hand, treatment of hydrophobic COCs such as chlorinated organics is enhanced due to the hydrophobicity and high electron transferability of S producing high electron selectivity and utilization through hydrophobic COCs. S-NZVI generates much more hydroxyl radicals for pollutant degradation through a one-electron transfer pathway than NZVI. Nevertheless, the simulation in this study focused on bulk FeS and not nanoscale FeS. Further modification of DFT-D2 to simulate nanoscale FeS is needed to accurately explain these findings on S-NZVI.

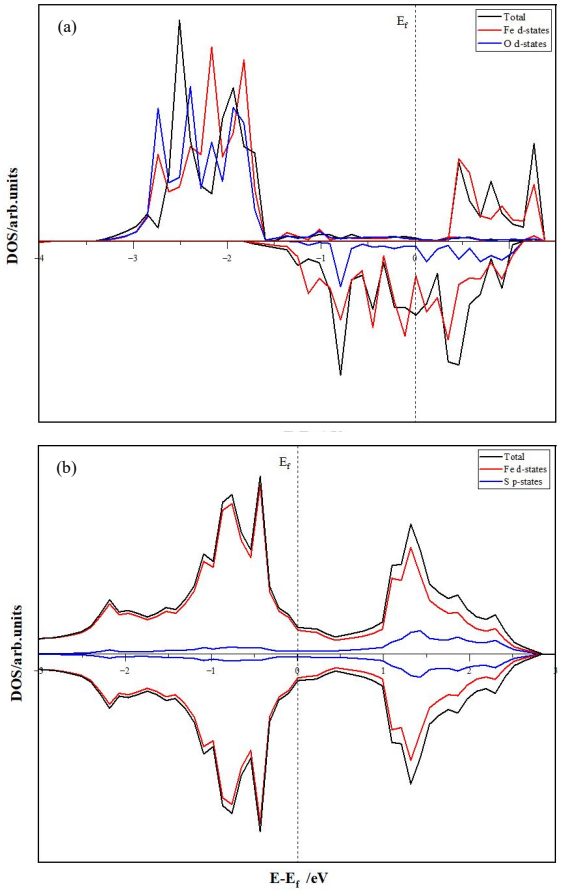

Figure. 6 DFT-D2(PBE) density of states of (a) Fe_3O_4 in the *Fd3m* unit cell and (b) FeS in the *P4/nmm* unit cell . The Fermi level (=zero of energy, see text) is shown as a dashed line.

5. CONCLUSION

We present a computational study of the inversion thermodynamics of the bulk and electronic band structure and density of states (DOS) of bulk Fe_3O_4 and FeS using first principles methods based on the density functional theory. Both DFT and DFT-D2 were implemented, and the results compared with previous experimental results. The simulated properties substantially agree with previous experimental results. Nevertheless, for both bulk Fe_3O_4 and bulk FeS, DFT-D2 performed better than DFT in terms of the accuracy of simulated unit cell parameters. Both DFT and DFT-D2 can also simulate the DOS of both materials effectively. The DOS of Fe_3O_4 supports electron transfer from the central octahedral-Fe_B layer to the outer tetrahedral-Fe_A layer, while the DOS of FeS potentially explains the decrease of the NZVI aging effect and enhanced treatment of hydrophobic contaminants due to sulfidation reported in the literature. This research illustrates that DFT and DFT-D2 can be tools of choice for further modification of interfacial Fe_3O_4 and FeS surface modeling, as well as their interaction with COCs at nanoscale for environmental engineering applications.

6. ACKNOWLEDGMENTS

This work was financially supported by the National Research Council of Thailand (NRCT5-RSA63011-01), 2) the Faculty of Engineering, Naresuan University, Phitsanulok, Thailand (to S. Tongkamnoi), and 3) the Nanostructure Computational Network (NCN) of College of Materials Innovation and Technology, King Mongkut's Institute of Technology Ladkrabang (to Mayuree P. Reilly). We also very much appreciate the permission to access high-performance computers at National e-Science Infrastructure Consortium by National Electronics and Computer Technology Center (NECTEC), Thailand.

7. REFERENCES

Barbieri, A., Weiss, W., Van Hove, M., & Somorjai, G. (1994). Magnetite Fe_3O_4 (111): surface structure by LEED crystallography and energetics. *Surface Science*, *302*(3), 259-279. https://doi.org/10.1016/0039-6028(94)90832-X

Berner, R. A. (1962). Tetragonal iron sulfide. *Science*, *137*(3531),669-669. https://doi.org/10.1126/science.137.3531.669.b

Blochl, P. E. (1994). Projector augmented-wave method. *Phys Rev B Condens Matter*, *50*(24), 17953-17979. https://doi.org/10.1103/physrevb.50.17953

Cornell, R. M., & Schwertmann, U. (2003). *The iron oxides: structure, properties, reactions, occurrences, and uses* (Vol. 664). Wiley-vch Weinheim. https://doi.org/10.1515/CORRREV.1997.15.3-4.533

Dahl, J., & Avery, J. (1986). *Local densityapproximations in quantum chemistry and solid state physics*.

De la Pierre, M., Orlando, R., Maschio, L., Doll, K., Ugliengo, P., & Dovesi, R. (2011). Performance of six functionals (LDA, PBE, PBESOL, B3LYP, PBE0, and WC1LYP) in the simulation of vibrational and dielectric properties of crystalline compounds. The case of forsterite Mg_2SiO_4. *J Comput Chem*, *32*(9), 1775-1784. https://doi.org/10.1002/jcc.21750

Devey, A., Grau-Crespo, R., & De Leeuw, N. (2008). Combined density functional theory and interatomic potential study of the bulk and surface structures and properties of the iron sulfide mackinawite (FeS). *The Journal of Physical Chemistry C*, *112*(29), 10960-10967. https://doi.org/10.1021/jp8001959

Dzade, N., Roldan, A., & de Leeuw, N. H. (2014). The surface chemistry of NO_x on mackinawite (FeS) surfaces: a DFT-D2 study. *Physical Chemistry Chemical Physics*, *16*(29), 15444-15456. https://doi.org/10.1039/C4CP01138D

Dzade, N. Y., Roldan, A., & De Leeuw, N. H. (2013). Adsorption of methylamine on mackinawite (FeS) surfaces: A density functional theory study. *The Journal of Chemical Physics*, *139*(12),124708. https://doi.org/10.1063/1.4822040

Fan, D., O'Brien Johnson, G., Tratnyek, P. G., & Johnson, R. L. (2016). Sulfidation of nano zerovalent iron (nZVI) for improved selectivity during in-situ chemical reduction (ISCR). *Environmental Science & Technology*, *50*(17), 9558-9565. https://doi.org/10.1021/acs.est.6b02170

Grimme, S. (2006). Semiempirical GGA-type density functional constructed with a long-range dispersion correction. *J Comput Chem*, *27*(15), 1787-1799. https://doi.org/10.1002/jcc.20495

Jeong, H. Y., Lee, J. H., & Hayes, K. F. (2008). Characterization of synthetic nanocrystalline mackinawite: crystal structure, particle size, and specific surface area. *Geochimica et cosmochimica acta*, *72*(2), 493-505. https://doi.org/10.1016/j.gca.2007.11.008

Kim-Ngan, N.-T., Soszka, W., & Kozłowski, A. (2004). Studies of an Fe_3O_4 (111) surface by low-energy ion scattering. *Journal of magnetism and magnetic materials*, *279*(1), 125-133. https://doi.org/10.1016/j.jmmm.2004.01.092

Kresse, G., & Furthmüller, J. (1996). Efficiency of ab-initio total energy calculations for metals and semiconductors using a plane-wave basis set. *Computational Materials Science*, *6*(1), 15-50. https://doi.org/10.1016/0927-0256(96)00008-0

Kresse, G., & Hafner, J. (1993). Ab initio molecular dynamics for liquid metals. *Phys Rev B Condens Matter*, *47*(1), 558-561. https://doi.org/10.1103/physrevb.47.558

Kresse, G., & Joubert, D. (1999). From ultrasoft pseudopotentials to the projector augmented-wave method. *Physical Review B*, *59*(3), 1758-1775. https://doi.org/10.1103/physrevb.59.1758

Labanowski, J. K., & Andzelm, J. W. (2012). *Density functional methods in chemistry*. Springer Science & Business Media. https://doi.org/10.1007/978-1-4757-0818-9_5

Lennie, A., Redfern, S. A., Schofield, P., & Vaughan, D. (1995). Synthesis and Rietveld crystal structure refinement of mackinawite, tetragonal FeS. *Mineralogical Magazine*, *59*(397), 677-683.

Lennie, A. R., Redfern, S. A., Champness, P. E., Stoddart, C. P., Schofield, P. F., & Vaughan, D. J. (1997). Transformation of mackinawite to greigite; an in situ X-ray powder diffraction and transmission electron microscope study. *American Mineralogist*, *82*(3-4), 302-309. https://doi.org/10.2138/am-1997-3-408

Liu, Y., Majetich, S. A., Tilton, R. D., Sholl, D. S., & Lowry, G. V. (2005). TCE dechlorination rates, pathways, and efficiency of nanoscale iron particles with different properties. *Environmental Science & Technology*, *39*(5), 1338-1345. https://doi.org/10.1021/es049195r

Liu, Y., Phenrat, T., & Lowry, G. V. (2007). Effect of TCE concentration and dissolved groundwater solutes on NZVI-promoted TCE dechlorination and H_2 evolution. *Environmental Science & Technology*, *41*(22), 7881-7887. https://doi.org/10.1021/es0711967

Mackenzie, K., & Georgi, A. (2019). NZVI synthesis and characterization. *Nanoscale Zerovalent Iron Particles for Environmental Restoration: From Fundamental Science to Field Scale Engineering Applications*, 45-95. https://doi.org/10.1007/978-3-319-95340-3_2

Marand, Z. R., Farimani, M. H. R., & Shahtahmasebi, N. (2014). Study of magnetic and structural and optical properties of Zn doped Fe_3O_4 nanoparticles synthesized by co-precipitation method for biomedical application. *Akush. Ginekol.(Sofiia)*, *15*, 238-247. https://doi.org/10.7508/NMJ.2015.04.004

Monkhorst, H. J., & Pack, J. D. (1976). Special points for Brillouin-zone integrations. *Physical Review B*, *13*(12), 5188-5192. https://doi.org/10.1103/physrevb.13.5188

Néel, L. (1984). Magnetic properties of ferrites: ferrimagnetism and antiferromagnetism. *Physical Chemical & Earth Sciences*(31), 18.

Perdew, J. P., Burke, K., & Ernzerhof, M. (1996). Generalized Gradient Approximation Made Simple. *Physical Review Letters*, *77*(18), 3865-3868. https://doi.org/10.1103/physrevlett.77.3865

Perdew, J. P., Chevary, J. A., Vosko, S. H., Jackson, K. A., Pederson, M. R., Singh, D. J., & Fiolhais, C. (1992). Atoms, molecules, solids, and surfaces: Applications of the generalized gradient approximation for exchange and correlation. *Phys Rev B Condens Matter*, *46*(11), 6671-6687. https://doi.org/10.1103/physrevb.46.6671

Phenrat, T., & Lowry, G. V. (2019). Nanoscale zerovalent iron particles for environmental restoration. *From Fundamental Science to Field Scale Engineering Applications*. https://doi.org/10.1007/978-3-319-95340-3

Phenrat, T., Schoenfelder, D., Kirschling, T. L., Tilton, R. D., & Lowry, G. V. (2018). Adsorbed poly (aspartate) coating limits the adverse effects of dissolved groundwater solutes on Fe^0 nanoparticle reactivity with trichloroethylene. *Environmental Science and Pollution Research*, *25*, 7157-7169. https://doi.org/10.1007/s11356-015-5092-4

Phenrat, T., Thongboot, T., & Lowry, G. V. (2016). Electromagnetic induction of zerovalent iron (ZVI) powder and nanoscale zerovalent iron (NZVI) particles enhances dechlorination of trichloroethylene in contaminated groundwater and soil: proof of concept. *Environmental Science & Technology*, *50*(2), 872-880. https://doi.org/10.1021/acs.est.5b04485

Politzer, P., Seminario, J. M., Concha, M. C., & Murray, J. S. (1993). Some applications of local density functional theory to the calculation of reaction

energetics. *Theoretica Chimica Acta*, *85*(1-3), 127-136. https://doi.org/10.1007/bf01374583

Reinsch, B. C., Forsberg, B., Penn, R. L., Kim, C. S., & Lowry, G. V. (2010). Chemical transformations during aging of zerovalent iron nanoparticles in the presence of common groundwater dissolved constituents. *Environmental Science & Technology*, *44*(9), 3455-3461. https://doi.org/10.1021/es902924h

Santos-Carballal, D., Roldan, A., Dzade, N. Y., & de Leeuw, N. H. (2018). Reactivity of CO_2 on the surfaces of magnetite (Fe_3O_4), greigite (Fe_3S_4) and mackinawite (FeS). *Philos Trans A Math Phys Eng Sci*, *376*(2110). https://doi.org/10.1098/rsta.2017.0065

Santos-Carballal, D., Roldan, A., Grau-Crespo, R., & de Leeuw, N. H. (2014). A DFT study of the structures, stabilities and redox behaviour of the major surfaces of magnetite Fe_3O_4. *Phys Chem Chem Phys*, *16*(39), 21082-21097. https://doi.org/10.1039/c4cp00529e

Su, Y., Lowry, G. V., Jassby, D., & Zhang, Y. (2019). Sulfide-modified NZVI (S-NZVI): synthesis, characterization, and reactivity. *Nanoscale Zerovalent Iron Particles for Environmental Restoration: From Fundamental Science to Field Scale Engineering Applications*, 359-386. https://doi.org/10.1007/978-3-319-95340-3_9

Subedi, A., Zhang, L., Singh, D. J., & Du, M.-H. (2008). Density functional study of FeS, FeSe, and FeTe: Electronic structure, magnetism, phonons, and superconductivity. *Physical Review B*, *78*(13), 134514. https://doi.org/10.1103/PhysRevB.78.134514

Sun, R., & Ceder, G. (2011). Feasibility of band gap engineering of pyrite FeS 2. *Physical Review B*, *84*(24), 245211.

Vanderbilt, D. (1990). Soft self-consistent pseudopotentials in a generalized eigenvalue formalism. *Phys Rev B Condens Matter*, *41*(11), 7892-7895. https://doi.org/10.1103/physrevb.41.7892

Vaughan, D., & Ridout, M. (1971). Mössbauer studies of some sulphide minerals. *Journal of Inorganic and Nuclear Chemistry*, *33*(3), 741-746. https://doi.org/10.1016/0022-1902(71)80472-4

Weiss, W., & Ranke, W. (2002). Surface chemistry and catalysis on well-defined epitaxial iron-oxide layers. *Progress in Surface Science*, *70*(1-3), 1-151. https://doi.org/10.1016/s0079-6816(01)00056-9

Wimmer, E. (1996). Computational materials design and processing: perspectives for atomistic approaches. *Materials Science and Engineering: B*, *37*(1-3), 72-82. https://doi.org/10.1016/0921-5107(95)01459-4

Xu, J., Li, H., & Lowry, G. V. (2021). Sulfidized nanoscale zero-valent iron: tuning the properties of this complex material for efficient groundwater remediation. *Accounts of Materials Research*, *2*(6), 420-431. https://doi.org/10.1021/accountsmr.1c00037

Yang, T., Wen, X.-d., Ren, J., Li, Y.-w., Wang, J.-g., & Huo, C.-f. (2010). Surface structures of Fe_3O_4 (111), (110), and (001): A density functional theory study. *Journal of Fuel Chemistry and Technology*, *38*(1), 121-128. https://doi.org/10.1016/s1872-5813(10)60024-2

Zhang, Z., & Satpathy, S. (1991). Electron states, magnetism, and the Verwey transition in magnetite. *Physical Review B*, *44*(24), 13319. https://doi.org/10.1103/PhysRevB.44.13319

8. Biographies

Saranya Tongkamnoi

Challenges in Environmental Science and Engineering (CESE2020) "Understanding surface structure properties and chemisorption of trichloroethylene (TCE) on sulfide-modified nanoscale zerovalent iron (S-NZVI) surfaces using density functional theory (oral presentation)"

ice.saran37@gmail.com

Mayuree P. Reilly

Material simulations for alternative energy and sensor applications, computational chemistry, ab initio and DFT calculation, reaction mechanisms on surfaces, structural, electronic structure, energetic, spectroscopic and dynamic properties of materials.

mayuree.ph@kmitl.ac.th

Tanapon Phenrat

Groundwater and soil remediation, nanomaterials for environmental restoration, groundwater modeling, site characterization, risk assessment.

pomphenrat@gmail.com